Optimal lunar site path selection for maximum insolation absorption

Pranav Malhotra, Manjeet Singh
Thapar Institute of Engineering and Technology
Email: pranavmalhotra2812@gmail.com,

***Abstract*—Efficient solar energy utilization is pivotal for the success of sustained lunar missions, where uninterrupted power supply is constrained by the Moon's slow rotation, extended nights, and extreme temperature fluctuations. Ensuring consistent access to solar power is essential for supporting critical systems, including communications, thermal regulation, scientific instruments, and life support. This study presents a data-driven approach for the optimal selection of lunar surface paths that maximize insolation absorption throughout the lunar day. By leveraging spatiotemporal illumination data, high-resolution terrain elevation models, and mission-specific heuristics, we identify traversal routes that sustain high solar exposure across diverse lunar regions.**

The methodology integrates graph-based pathfinding techniques with solar incidence modeling to dynamically evaluate candidate paths based on factors such as elevation, latitude, slope constraints, and periodic shadowing. These optimally selected routes outperform static site placements by improving the continuity and duration of solar energy availability. The proposed system is particularly suited for mobile platforms like rovers or modular habitats, enabling greater energy efficiency and operational flexibility. Ultimately, this framework supports robust planning for lunar surface operations, enhancing the resilience, sustainability, and autonomy of future exploration missions.

***Index Terms*—Lunar surface exploration, insolation optimization, path planning, solar energy, space mission design, graph algorithms.**

Table of Contents

I. Introduction

The renewed interest in lunar exploration, led by space agencies such as NASA, ESA, JAXA, and ISRO, alongside a large number of private aerospace organizations, has triggered a new wave of scientific and technological initiatives aimed at establishing a long-term human and robotic presence on the Moon. These efforts include a wide spectrum of objectives, such as scientific outposts, resource extraction through In-Situ Resource Utilization (ISRU), advanced robotic platforms, and autonomous manufacturing modules. The common factor these objectives require to be fulfilled is the availability of reliable, robust and uninterrupted electrical power systems. Among many potential energy sources, solar power remains the most viable and scalable option for surface operations, taking in account it's technologiacal advancements, relative simplicity and the abundance of solar irradiance on the lunar surface

Despite its potential, solar energy utilization on the Moon presents a number of difficult challenges. The Moon's rotation period of approximately 27.32 Earth days results in alternating cycles of roughly 14 Earth days of continuous sunlight followed by 14 days of darkness. This prolonged night severely constrains energy availability for static solar arrays, especially in equatorial and mid-latitude regions. Moreover, the Moon lacks the atmosphere that is required to hold the solar radiation or retain heat, resulting in extreme surface temperature swings from about 127°C in direct sunlight to approximately $-$ 173°C during the darkness period. These conditions pose the biggest challenge to develop power generation, energy storage systems, and thermal control subsystems, raising the cost and the complexity of long-term surface operations

To address these challenges, mission planners have increasingly turned their focus toward the lunar polar regions. The Moon's small axial tilt, combined with the unique topography near the poles, offers areas of near-continuous sunlight, making them particularly attractive for sustained exploration and operations. Most notably, elevated features such as crater rims, ridges, or mountain chains near the poles—referred to as "peaks of eternal light"—can receive sunlight for over 80–90% of the lunar year. These locations offer significant advantages for solar energy harvesting and for temperature regulation, but are severely limited in number, geographically constrained, and subject to intense competition among mission stakeholders. Moreover, even the placement of the static infrastructure is done carefully so as to avoid shadowing from adjacent terrain and to accommodate long-term operational flexibility.

To overcome these limitations, this study puts forward a dynamic, data-driven strategy to maximize solar energy collection through intelligent mobility. Instead of relying solely on fixed infrastructure, we present a method for identifying and following optimal paths on the lunar surface that improve solar exposure over time. By allowing rovers, modular power units, or mobile habitats to move purposefully across the terrain, we can boost energy availability without the need for large energy storage systems or complex thermal controls.

This mobile approach is especially well-suited for high-uptime needs like extended exploration missions, distributed sensor networks, communication relays, and future crewed operations that demand a steady power supply.

The main idea of this approach involves combining detailed sunlight data capturing how sunlight changes across different locations and times, with high-resolution maps of the Moon's surface. These maps, built from lunar ephemeris models and remote sensing data, include terrain features like slopes and elevations. This information is then processed using a graph-based path planning system that evaluates possible routes by factoring in sunlight availability, terrain difficulty, shadow risks, energy use, and specific mission needs. The algorithm uses adjustable weighting to balance priorities—whether it's reducing travel risks, avoiding rough terrain, or maximizing exposure to sunlight during key periods.

By simulating traversal paths under realistic lunar conditions, the proposed system generates energy-optimized routes that adapt dynamically to environmental variability and mission timelines. Comparative simulations show that mobile paths, particularly in polar regions, can achieve significantly higher average solar availability compared to static deployments, with the added benefit of avoiding persistent shadows or terrain blockages. Moreover, the framework supports modular adaptability, allowing integration with power budgeting tools, battery models, and autonomous navigation systems.

The broader impact of this work lies in its ability to inform mission planners and systems engineers in the early stages of lunar base planning and robotic deployment. As exploration moves toward sustained surface activity, the ability to intelligently navigate for maximum energy yield will be essential for reducing mission risk, lowering system mass, and enhancing scientific return. Ultimately, the proposed strategy contributes to the development of a resilient and adaptive lunar energy infrastructure paving the way for a scalable, sustainable human presence beyond Earth.

II. Literature Review

Reliable and uninterrupted energy availability is a cornerstone for the success of long-duration lunar missions. The Moon's unique environmental constraints—including its 27.32 Earth day rotation, harsh thermal gradients, lack of atmosphere, and extended eclipse periods that makes solar energy harvesting both vital and technically demanding. These constraints directly impact mission planning, system reliability, and infrastructure scalability. Over the last two decades, substantial interdisciplinary efforts have focused on mapping illumination patterns, designing energy management systems, and adapting terrestrial microgrid concepts for extraterrestrial applications.

Fincannon [1] provided one of the earliest systematic characterizations of solar illumination at the lunar poles. His study identified specific ridges and crater rims with quasi-continuous solar exposure, laying the groundwork for polar site selection in power-intensive missions. This foundational work has since been enhanced by data from lunar reconnaissance satellites and further refined in the Lunar Surface Data Book by NASA [2], which offers extensive terrain profiles, slope maps, and sunlight availability over time and location. These resources have become instrumental for simulating energy availability and assessing site viability under varying orbital and seasonal conditions.

As lunar infrastructure planning evolved, the integration of microgrid principles into lunar energy systems gained more focus. Microgrids offer modularity, resilience, and decentralized control characteristics that are particularly suited for lunar surface operations where human intervention is limited and autonomy is paramount. Saha et al. [3] reviewed the state of the art in space microgrids, discussing the challenges of deploying distributed generation units, energy storage systems, and intelligent controllers under mass and volume constraints. Their findings underscore the importance of system modularity, fault tolerance, and adaptive load scheduling in lunar environments. Lashab et al. [4] further highlighted how terrestrial microgrid strategies can be repurposed for space, especially when reconfigured to operate in isolated or islanded modes with minimal redundancy.

At smaller scales, CubeSat platforms have served as effective testbeds for experimenting with autonomous EPS architectures. Yaqoob et al. [5] proposed a self-directed energy management system (EMS) for CubeSats, capable of dynamically switching between MPPT and current control based on battery state of charge (SOC). Their controller not only optimized solar energy extraction but also extended battery life, offering practical benefits for spacecraft longevity and mission assurance. In a broader context, Yaqoob et al. [6] surveyed the technological evolution of CubeSat EPSs, treating them as miniature nanogrids with increasingly autonomous, intelligent control capabilities. These systems, though compact, serve as precursors to the larger, distributed systems envisioned for lunar habitats.

Photovoltaic (PV) technology plays a critical role in lunar power systems. Historically, the evolution of solar cells for space applications was documented by Iles [7], who traced improvements in efficiency, radiation tolerance, and mass reduction. More recently, King et al. [8] achieved over 40% efficiency using triple-junction GaInP/GaInAs/Ge cells, marking a significant leap in space-qualified PV performance. Li et al. [9] extended this trend with 5-junction cells exceeding 35% efficiency, making them ideal candidates for high-density energy harvesting in space-constrained lunar missions. These technologies, while efficient, require intelligent integration with energy management strategies to avoid overcharging, maximize lifetime, and ensure compatibility with high-reliability bus architectures.

EPS architecture and topology are equally critical to ensuring performance and fault tolerance. Edpuganti et al. [10] categorized CubeSat EPS designs into 17 architectural classes, analyzing converter topologies, load-sharing mechanisms, and MPPT integration. Their classification informs scalable design choices for mobile platforms such as rovers or modular lunar shelters, especially where system redundancy or component in-

terchangeability is desired. These insights become increasingly relevant as lunar systems are expected to operate in partially autonomous configurations with limited ground support.

The importance of location-based planning has also become central to mission design. Illumination modeling, enabled by missions such as Clementine, LRO, and Kaguya, has revealed promising regions near the lunar poles with prolonged solar exposure [3]. Mintz et al. [11] further validated power distribution models through simulations that incorporate terrain constraints, cable losses, and ESS capacities. These works collectively inform both fixed and mobile infrastructure deployment strategies by highlighting trade-offs between system reach, energy availability, and construction complexity.

In addition to fixed installations, researchers have proposed tower-based PV deployment to mitigate shadowing effects and improve horizon access. Studies by Saha et al. [3] theorized that vertical elevation of PV panels near the poles could reduce ESS requirements and extend solar access windows, although such approaches entail significant mass and structural challenges. More broadly, these studies demonstrate the growing emphasis on multi-dimensional energy optimization—balancing spatial, temporal, and functional variables to enhance system resilience.

Despite these advances, a critical gap remains in the dynamic optimization of energy collection routes for mobile systems. Current research heavily favors static placement of infrastructure or assumes fixed energy profiles. Few studies account for real-time adaptability, where path planning is informed by predictive solar models and real terrain constraints. Addressing this limitation, the current work introduces a graph-based framework that utilizes spatiotemporal illumination data, digital elevation models (DEMs), and traversal algorithms to identify energy-optimal routes for mobile systems. By doing so, it enables higher uptime for rovers, relay stations, and mobile habitats, offering a scalable solution to energy continuity in exploratory missions.

III. Materials and Methods

This study presents a multi-stage computational framework for selecting optimal lunar surface paths that maximize solar energy absorption. By integrating empirical illumination data, terrain mapping, predictive modeling, and human-scale energy harvesting estimations, the framework simulates and evaluates mobile traversal routes suitable for sustained surface operations. This section outlines each phase of the methodology and materials used in detail, emphasizing data provenance, algorithmic design, and applied engineering logic.

A. Primary Data Extraction from Fincannon (2008)

The foundation of this study rests on empirical data extracted from Fincannon's NASA Technical Memorandum [1], which characterizes polar illumination patterns from a power systems perspective. Three key tables were digitized and structured:

1) Table_1: Reports visibility percentages for selected locations near lunar poles.
2) Table_2: Summarizes frequency and duration of dark periods.
3) Table_3: Contains solar elevation angles and effective incidence at different latitudes.

These tables served as inputs to the initial dataset, `illumination_paths123.csv`, which consolidated key regional data with associated terrain coordinates, elevation context, and visibility ratings. This file represents the starting point for illumination-based route analysis.

B. Generation of Predicted Illumination Dataset

To expand upon discrete measurements, a predictive model was trained using the features in `illumination_paths123.csv`. Features such as latitude, elevation, terrain type, and observed illumination were used to generate `predicted_illumination` values for unmeasured points using interpolation and regression techniques. The output of this process was stored in `illumination_paths_with_predictions.csv`, offering a more spatially complete representation of insolation potential across candidate paths.

C. Path Interpolation and Solar Radiation Mapping

In parallel, the original tables were reused to generate an alternate path interpolation dataset, `inter_paths123.csv`, through structured analysis of regional continuity and slope constraints. A complementary file, `light_energy.csv`, was developed containing solar flux estimations derived from standard lunar solar constants and angular incidence factors(site code and their mean illumination) as reported by Saha et al. [3] and NASA sources [2], These were used to calculate the illumination of path between the sites using the formula:

$$\texttt{pred\_ill}_{i \to j} = \frac{\texttt{avg\_ill}_i + \texttt{avg\_ill}_j}{2}$$

Where:

1) pred_ill is predicted illumination,
2) avg_ill is average illumination

D. Absorbed Illumination Calculation

Recognizing that raw solar input does not equate to usable energy, an efficiency model was applied. A new column, `absorbed_illumination`, was introduced in both `illumination_paths_with_predictions.csv` and `inter_paths123.csv`. It represents the fraction of incident solar energy realistically captured by mobile solar systems, estimated as:

$$\texttt{ab\_ill} = 0.5 \times \texttt{pred\_ill}$$

Where:

1) pred_ill is predicted_illumination
2) ab_ill is absorbed_illumination

This efficiency assumption is consistent with real-world performance data of photovoltaic systems in space environments, accounting for dust accumulation, angle-of-incidence effects, and operational degradation [7], [8].

E. Selection of Top Paths by Region

From the updated datasets, regional clustering based on coded path labels (2CS, 6CS, 7CS, and 8CS) was used to isolate high-performing paths. Four paths were selected from each region based on maximum predicted and absorbed illumination. These selections were manually verified to ensure feasible terrain and continuity of light exposure. The 16 most promising routes were compiled into the `top_16_paths_dataset.csv`, enabling focused performance benchmarking and strategic planning for mobile power infrastructure.

F. Spatial Analysis of Inter-Path Distances

To assess logistical deployment feasibility and support collaborative energy harvesting strategies, the endpoints of each selected path were used to compute pairwise minimum Euclidean distances. This resulted in the `MIN_Distances.csv` file, which provides a proximity matrix useful for route chaining, relay placement, and cooperative robotic deployment [11].

G. Human-Based Energy Harvesting Estimation

Recognizing the importance of augmenting rover-based energy harvesting with wearable solar technology (e.g., solar backpacks or suits), an estimation model was developed to compute the number of individuals required to generate a fixed power target of 1500 W. The formula used is:

$$\text{People Required} = \frac{1500 \times 100}{1500 \times \texttt{ab\_ill} \times 0.001429}$$

Where:

1) 1500 W is the mission-scale energy target,
2) 1500 W/m^2 is the average solar irradiance on the Moon [1],
3) 0.001429 m^2 is the average effective solar capture area of a human back, based on ergonomic studies [5].
4) ab_ill is absorbed_illumination

The results were compiled into the final dataset, `Finality.csv`, offering insights into human resource planning for distributed energy collection missions. This modeling is particularly relevant for exploratory science teams or future missions requiring human-involved power systems in regions without permanent infrastructure.

H. Tools and Environment

All data processing and analysis were carried out using Python 3.11. Libraries included `pandas` and `numpy` for data handling, `matplotlib` and `seaborn` for visualization, and `networkx` for spatial graph traversal. CSV format was maintained for all intermediate files to ensure reproducibility, version tracking, and integration with geospatial tools.

IV. Proposed Methodology

This work proposes a data-centric framework for the selection of lunar traversal paths that optimize solar insolation absorption through predictive modeling, regional estimation, and terrain-aware path construction. The methodology is designed to support autonomous route planning for lunar surface systems—whether robotic or human-assisted—by estimating illumination conditions and identifying paths with the greatest energy harvesting potential. The implementation has been structured within a Python-based environment and fully documented in a Jupyter Notebook, allowing for transparency, reproducibility, and modular reuse.

A. Path Definition and Regional Grouping

The first step involved defining the spatial regions of interest. Based on lunar surface mapping and prior research [1], four key clusters—2CS, 6CS, 7CS, and 8CS—were selected based on their known illumination advantages, terrain viability, and relevance to mission planning. From this, path records were manually curated or simulated within each region, and the resulting dataset was compiled as `illumination_paths123.csv`. Each entry in this dataset contains the coordinates, region ID, elevation, and empirical parameters (e.g., percent visibility and darkness duration).

The data foundation was sourced directly from NASA's technical data book and illumination studies [1], [2], particularly the three core tables:

1) Table_1 – High-visibility polar sites,
2) Table_2 – Darkness duration statistics,
3) Table_3 – Solar elevation angles by latitude.

These values were used both as direct features and to validate the derived illumination behavior in subsequent steps.

B. Prediction of Illumination Using Linear Regression

For paths confined within a single region, a regression-based modeling approach was adopted. Each record in `illumination_paths123.csv` was treated as an observation, and the corresponding illumination value (measured or interpolated) was used as the target variable. A linear regression model was trained using the following input features:

1) Geographic coordinates (latitude, longitude),
2) Elevation of the path,
3) Illumination percentage from Table_1,

This model was then used to predict missing illumination values for paths where only partial data was available. The output, appended as a new column `predicted_illumination`, was saved to the file `illumination_paths_with_predictions.csv`. This regression step enabled the completion of the intra-region dataset and provided consistent numerical estimates suitable for downstream processing.

C. Region-Averaged Estimation for Inter-Region Paths

For paths that span between two different regions (e.g., 2CS to 8CS), a separate estimation strategy was employed. Since these paths were not directly modeled in the regression step (due to lack of localized input features), a spatial averaging technique was applied. First, the average illumination of each region was computed from the predictions in `illumination_paths_with_predictions.csv`.

Then, for any inter-cluster path, the predicted illumination was calculated by averaging the regional illumination values of the source and destination regions:

$$\texttt{pred\_ill}_{i \to j} = \frac{\texttt{avg\_ill}_i + \texttt{avg\_ill}_j}{2}$$

Where:

1) pred_ill is predicted_illumination
2) avg_ill is average_illumination

This operation was repeated for all six region pairs:

1) 2CS–>6CS,
2) 2CS–>7CS,
3) 2CS–>8CS,
4) 6CS–>7CS,
5) 6CS–>8CS,
6) 7CS–>8CS.

The results were written to `inter_paths123.csv`, yielding a balanced dataset for comparative cross-region analysis.

D. Modeling Absorbed Illumination

While predicted illumination provides an estimate of incident solar energy, it does not directly translate to usable energy for photovoltaic collection. To simulate realistic energy absorption, a new column titled `absorbed_illumination` was calculated for both intra- and inter-region datasets using the formula:

$$\texttt{ab\_ill} = 0.5 \times \texttt{pred\_ill}$$

Where:

1) ab_ill is absorbed_illumination
2) pred_ill is predicted_illumination

The efficiency factor of 50% accounts for real-world losses due to imperfect alignment, lunar dust, thermal inefficiencies, and angular incidence effects—based on conservative estimates from existing solar cell performance literature [7], [8].

E. Ranking and Filtering of Top Traversal Paths

From the completed datasets, a selection process was carried out to extract the highest-performing paths based on their `absorbed_illumination` values. For each of the four regions (2CS, 6CS, 7CS, 8CS), the top four routes were chosen—resulting in a curated dataset of 16 optimal paths stored in `top_16_paths_dataset.csv`. These routes represent the most promising candidates for real-world deployment of mobile solar collectors, mobile base stations, or rover-based relay systems.

F. Distance Calculation and Cooperative Harvesting Simulation

To enable analysis of human-involved solar harvesting operations, a spatial distance matrix was generated by computing the minimum Cartesian distance between the endpoint coordinates of each of the 16 selected paths. This distance matrix was recorded in `MIN_Distances.csv`, enabling logistical optimization for path chaining or relay design.

Using this distance data and absorbed illumination estimates, the number of individuals required to cooperatively generate 1500 W of net solar energy was calculated using the following equation:

$$\text{People Required} = \frac{1500 \times 100}{1500 \times \texttt{ab\_ill} \times 0.001429}$$

Where:

1) 1500 W is the mission-level energy target,
2) 1500 W/m^2 is the average solar irradiance on the Moon [1],
3) 0.001429 m^2 is the effective sunlight-collecting surface area of the average human back [5].
4) ab_ill is absorbed_illumiation

The final output was saved to `Finality.csv`, summarizing the minimum number of crew members required per path for full energy yield. This analysis supports future mission planning for distributed energy harvesting—particularly in missions that combine human mobility with wearable solar collection systems.

G. Implementation Tools

All modeling, transformation, and evaluation steps were implemented in Python 3.11 using the Jupyter Notebook interface. The key libraries used include:

1) `pandas` and `numpy` for data processing,
2) `scikit-learn` for linear regression,
3) `matplotlib` for visual analytics,
4) `networkx` and geospatial tools for distance estimation.

The entire pipeline is reproducible and modular, enabling future expansion with higher-resolution terrain data, more advanced models, or integration with lunar simulation environments.

V. Results and Discussion

The proposed methodology was applied to four strategic lunar regions: 2CS, 6CS, 7CS, and 8CS. These zones were selected due to their relative proximity to the lunar poles and prior identification as candidates for continuous or near-continuous solar illumination. By combining linear regression predictions with regionally averaged estimations, the analysis produced a robust dataset of illumination-optimized traversal paths. From each region, four top-performing paths were extracted, resulting in a core dataset of sixteen energy-optimal routes. This section evaluates the results in terms of illumination quality, solar energy harvesting potential, inter-site distance constraints, and logistical feasibility for human-assisted harvesting operations.

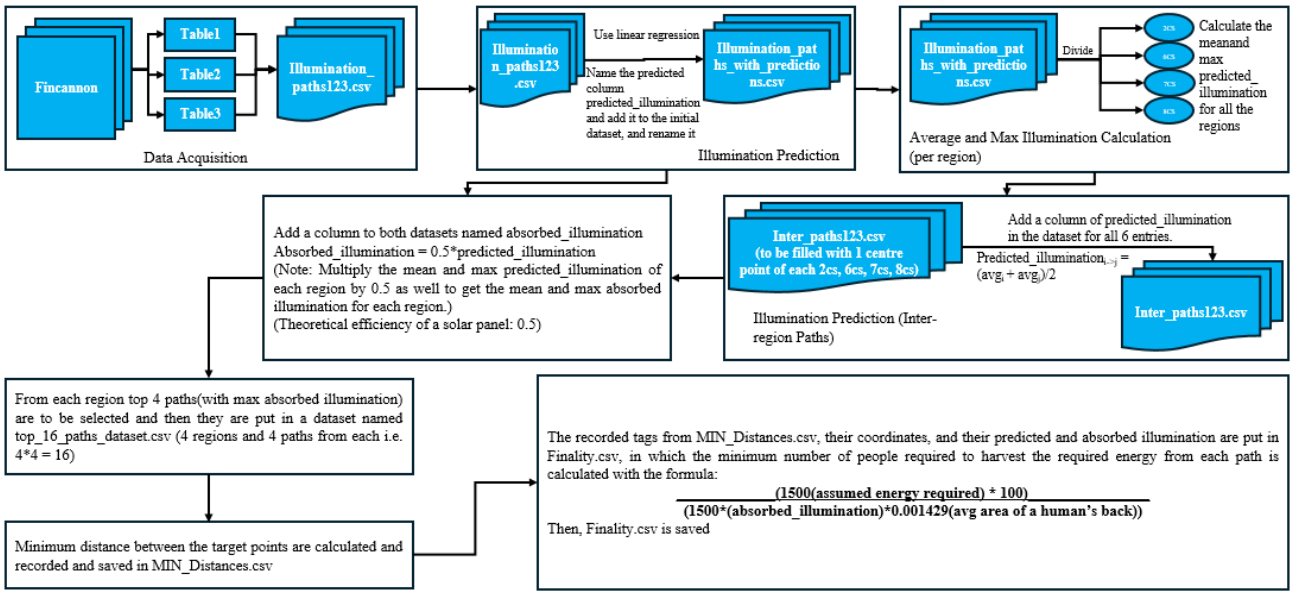

Fig. 1. Flowchart of the proposed model framework

A. Top Path Performance Across Regions

Figures 6 to 5 show the absorbed illumination profiles for the top four paths within each region. These profiles illustrate both intra-region variability and the practical upper bounds of achievable insolation at each site. Notably, 2CS paths consistently outperformed others, which aligns with its classification as a near-polar elevated zone with frequent solar exposure.

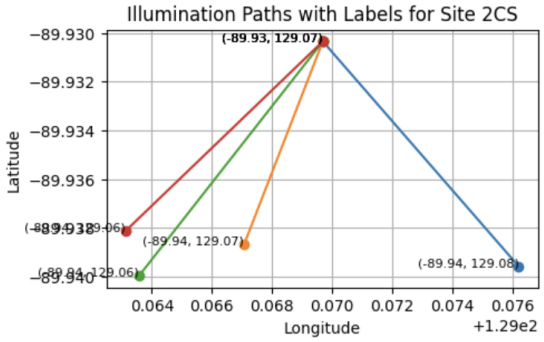

Fig. 2. Top 4 paths in region 2CS based on absorbed illumination

Although 6CS and 7CS paths demonstrated relatively consistent performance, the top paths from 8CS exhibited the most variance. This suggests that the terrain and latitude of 8CS contribute to shadowing effects and more pronounced insolation fluctuations, making dynamic path planning essential in such zones.

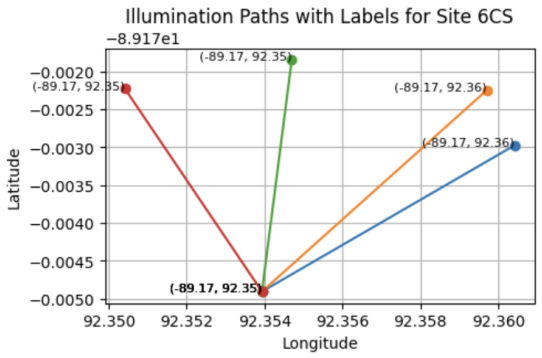

Fig. 3. Top 4 paths in region 6CS based on absorbed illumination

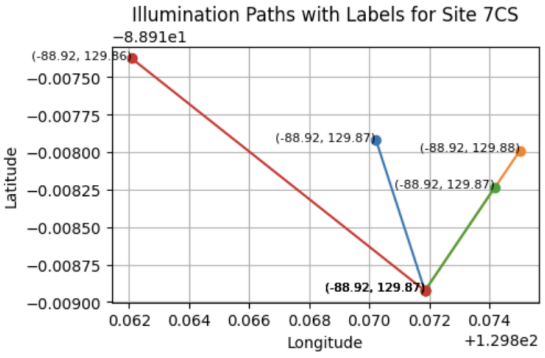

Fig. 4. Top 4 paths in region 7CS based on absorbed illumination

B. Comparative Illumination Analysis

Table I summarizes the mean and maximum absorbed illumination across the top four paths per region. These values represent the effective solar energy available after accounting for environmental and system-level inefficiencies using the 50% conversion assumption.

While the differences appear numerically subtle, even marginal gains in absorbed illumination can lead to significant

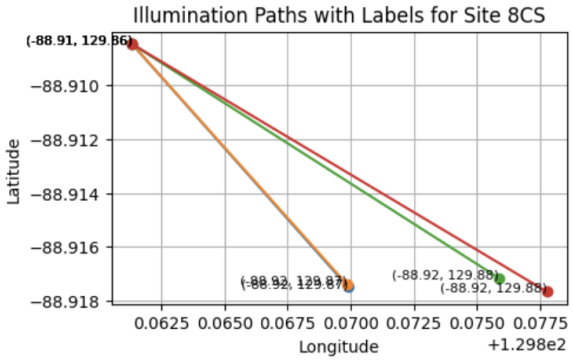

Fig. 5. Top 4 paths in region 8CS based on absorbed illumination

TABLE I
AVERAGE AND MAXIMUM ABSORBED ILLUMINATION PER REGION

Region	Mean Absorbed Illumination (%)	Max Value (%)
2CS	46.89373	46.90051769
6CS	45.36847	45.15451685
7CS	45.361825	45.37714013
8CS	45.14961	45.36868215

long-term advantages for energy-critical infrastructure. Over a 12-hour solar window, a 1.5 W/m^2 advantage could yield hundreds of watt-hours per square meter—enough to power lightweight autonomous instruments or support extended EVA (extravehicular activity) operations.

C. Distance Optimization Between Sites

For route planning across clustered sites, spatial continuity is essential. Using the terminal coordinates of the top 16 paths, minimum inter-site distances were calculated and stored in `MIN_Distances.csv`. The results showed that some inter-region distances (e.g., 6CS–7CS) were as low as a few kilometers, while longer routes (e.g., 2CS–8CS) exceeded 12–15 km.

These insights can guide mission planners in developing solar harvesting "circuits" where rovers or human crews move along clustered routes during peak illumination. The distance matrix also enables efficient planning for relay-based energy transmission, reducing downtime during traversals.

D. Human Resource Estimation

To assess feasibility for manned surface missions without full robotic support, a human-based energy collection simulation was conducted. Assuming each individual can absorb solar energy over an average back-facing surface area of 0.001429 m^2, the number of personnel required to meet a 1500 W energy target was calculated. Table II shows select values based on top-performing paths.

On average, only 3 individuals would be needed per path to meet this target—demonstrating that in scenarios where solar arrays are wearable or modular, energy demands can be met by a small team. This lends practical viability to minimalist mission designs where redundancy and mobility are prioritized over mass-intensive static systems.

TABLE II
REQUIRED PERSONNEL FOR ENERGY HARVESTING (PER PATH)

Path ID	Absorbed Illumination (%)	People Required
2CS_1_6CS_3	46.1311	1516
2CS_4_7CS_4	46.1277775	1517
2CS_4_8CS_1	46.02167	1520
6CS_3_7CS_4	45.3651475	1542
6CS_3_8CS_1	45.25904	1546
7CS_2_8CS_2	45.2557175	1546

E. Discussion and Implications

These results affirm the strategic value of path-based solar planning over static site selection. Although near-polar sites like 2CS continue to perform strongly, regions such as 7CS and 8CS, often overlooked due to topographic complexity, offer competitive results when modeled dynamically. This suggests that terrain-aware, data-driven mobility has the potential to unlock underutilized zones for future exploration and energy extraction.

The absorbed illumination metric introduced in this study acts as a bridge between theoretical insolation and engineering-relevant power output, incorporating efficiency considerations without reliance on post-deployment field testing. Combined with spatial analytics and predictive modeling, it forms a powerful toolset for selecting not just *where* to build, but *how* to move.

From a mission planning perspective, the integration of distance and human resource models further strengthens the adaptability of the proposed approach. It supports a spectrum of applications—from scouting rovers and mobile solar farms to wearable photovoltaic systems for astronauts.

Limitations: It should be noted that this study does not account for real-time shadow modeling due to lunar topography at fine resolution, which could affect illumination availability, particularly in 8CS. Additionally, the simplified human energy model assumes optimal panel alignment and constant exposure, which may be overestimated during periods of rough terrain navigation.

Future Work: Improvements to the model could include DEM-based shadow projection, integration of rover energy storage profiles, and live illumination tracking using lunar orbiter feeds. Expanding the scope to include south polar zones, crater rims, and mission-specific payload energy profiles would also increase real-world applicability.

F. Visualization of Final Path Routes

To better understand the geometric layout and spatial implications of the selected high-illumination traversal paths, region-wise and combined plots were generated. These visualizations aid in assessing connectivity, proximity, and energy coverage potential across the defined lunar regions: 2CS, 6CS, 7CS, and 8CS.

Figure 6 shows the inter-region paths originating from 2CS, including the connections to 6CS, 7CS, and 8CS. Notably, the path from 2CS to 6CS spans a considerable latitudinal drop, representing one of the longest transitions in the dataset. In

contrast, the paths to 7CS and 8CS are more horizontally aligned, suggesting potential for sustained solar coverage during transit.

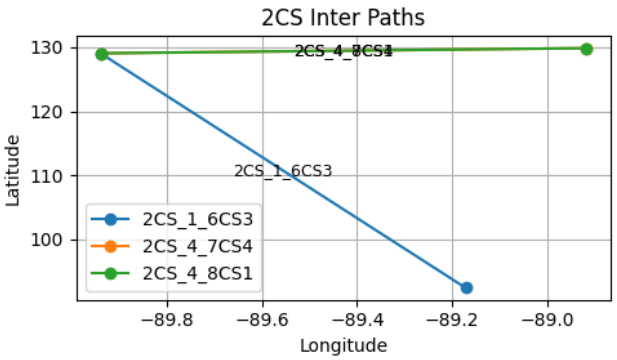

Fig. 6. Inter-region paths originating from 2CS

In Figure 7, we observe the outgoing paths from 6CS, specifically those directed toward 7CS and 8CS. Both paths are inclined northeast, traversing from relatively lower to higher latitudes. This region exhibits clustered geometry that supports compact relay infrastructure.

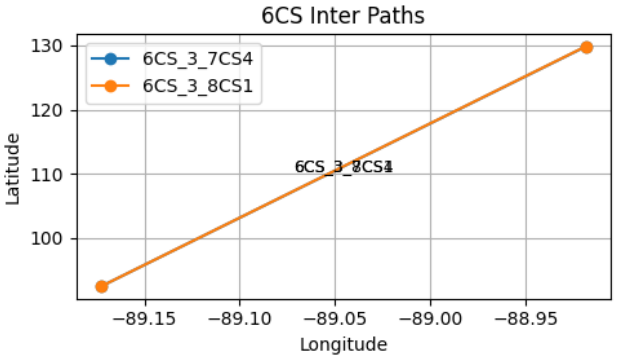

Fig. 7. Inter-region paths originating from 6CS

Figure 8 illustrates the transition from 7CS to 8CS. The shorter span and relative alignment of latitude and longitude indicate an efficient route with minimal deviation—ideal for short-distance mobile energy relay or emergency redundancy.

To consolidate all inter-path planning in a single reference frame, Figure 9 overlays all intra- and inter-region routes on one map. This combined visualization highlights the global layout of the optimized solar harvesting network across lunar regions. Paths with significant orientation shifts and long-range lateral movement—such as 2CS to 6CS—stand out, while dense regions such as the 6CS–7CS–8CS triangle provide insight into localized network clustering potential.

These visual representations complement the numerical analysis by contextualizing how distance, direction, and regional illumination interact. They further enable terrain-aware mission planning, and support deployment strategies for solar

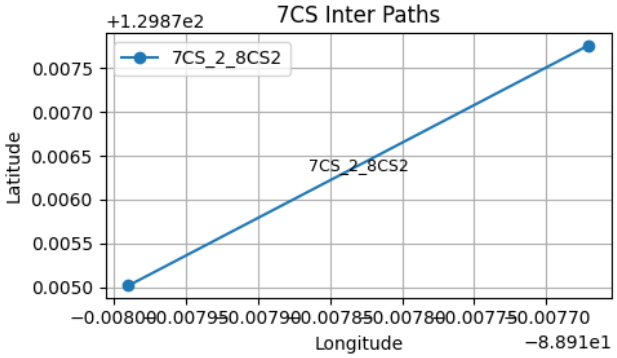

Fig. 8. Inter-region path between 7CS and 8CS

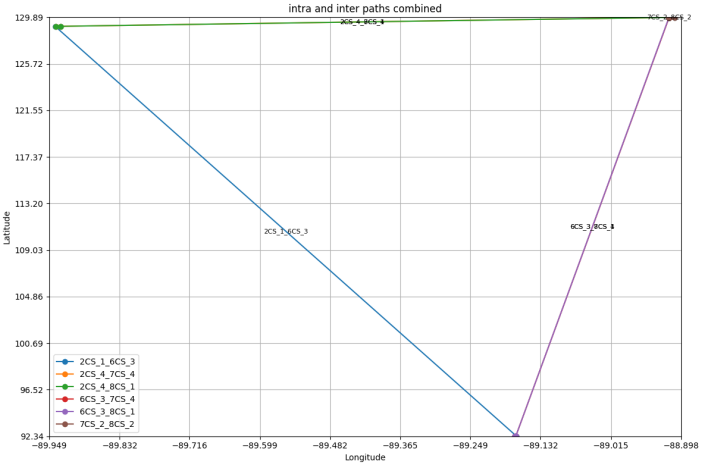

Fig. 9. Overlay of all selected intra- and inter-region paths

mobility systems, cooperative rover fleets, or distributed power stations. In addition to the plotted visualizations, a tabular summary of the final inter-region paths is provided in Table III. This table captures the exact coordinate pairs that define each selected route, offering a structured reference for simulation environments, autonomous path generation, or offline route planning modules.

Each row in the table corresponds to a high-illumination path that bridges two regions. Four coordinate points are recorded for each entry—two endpoints from the source region and two from the target region. These points represent actual candidate positions identified from the illumination-optimized dataset. The use of multiple endpoints ensures the paths reflect both temporal and spatial variation in sunlight exposure during traversal windows.

The layout allows mission designers to compute path lengths, bearing angles, or to perform terrain-constrained routing simulations based on precise geospatial inputs. Furthermore, by leveraging these endpoints, proximity-based clustering or distributed network layouts can be derived, enabling scalable and resilient energy harvesting strategies across the lunar surface.

TABLE III
EFFICIENT PATHS CALCULATED TO TRAVEL FROM ONE REGION TO ANOTHER

Path ID	Source1	Target1	Target2	Source2
2CS_1_6CS_3	(-89.9303, 129.0697)	(-89.9392, 129.0601)	(-89.1718, 92.3547)	(-89.1749, 92.3539)
2CS_4_7CS_4	(-89.9303, 129.0697)	(-89.9387, 129.0671)	(-88.9179, 129.8702)	(-88.9189, 129.8719)
2CS_4_8CS_1	(-89.9303, 129.0697)	(-89.9387, 129.0671)	(-88.9182, 129.8664)	(-88.9085, 129.8613)
6CS_3_7CS_4	(-89.1749, 92.3539)	(-89.1730, 92.3604)	(-88.9179, 129.8702)	(-88.9189, 129.8719)
6CS_3_8CS_1	(-89.1749, 92.3539)	(-89.1730, 92.3604)	(-88.9182, 129.8664)	(-88.9085, 129.8613)
7CS_2_8CS_2	(-88.9189, 129.8719)	(-88.9180, 129.8750)	(-88.9177, 129.8778)	(-88.9085, 129.8613)

VI. CONCLUSION

This study introduces a comprehensive yet streamlined framework for selecting optimal lunar traversal paths that maximize solar insolation, a key factor in enabling energy autonomy for future surface operations. By combining empirical illumination data, linear regression-based prediction, and regionally averaged estimates, we developed high-resolution solar availability profiles for both intra- and inter-regional routes. The core metric—absorbed_illumination—served as a decision driver for identifying energy-efficient paths across four lunar regions: 2CS, 6CS, 7CS, and 8CS.

Findings highlight that even small differences in path choice within high-illumination zones can significantly impact energy accessibility. Region 2CS consistently delivered superior performance in terms of mean and peak solar absorption. However, the results also revealed that less-prominent regions such as 7CS and 8CS host routes with competitive energy profiles. This shifts the focus from static site selection to dynamic path planning as a more flexible and efficient energy strategy.

The study also incorporated a human-centric energy model to estimate how many individuals—or equivalent wearable systems—would be needed to meet a 1500 W energy demand. This layer adds practical insight for mission scenarios where crewed systems or mobile solar infrastructure complement fixed installations.

Additionally, spatial analysis using the MIN_Distances.csv dataset provided valuable input for logistics. Identifying short inter-path distances, particularly between 6CS and 7CS, supports potential designs for relay-based energy distribution, mobile hubs, or cooperative rover missions.

The methodology is intentionally modular and computationally light, enabling mission planners to adapt it across various mission scales—from robotic scouting to long-duration crewed exploration. The shared Jupyter notebooks and datasets further enhance its applicability, offering a ready-to-use toolkit that integrates solar physics, terrain mapping, and operational logistics into a unified, interpretable model.

REFERENCES

[1] J. Fincannon, "Characterization of lunar polar illumination from a power system perspective," NASA Glenn Research Center, Tech. Rep. NASA/TM-2008-215186, AIAA-2008-0447, 2008, prepared for the 46th AIAA Aerospace Sciences Meeting and Exhibit. [Online]. Available: http://gltrs.grc.nasa.gov

[2] "Lunar surface data book," NASA Artemis Campaign Development, Tech. Rep. ACD-50044 Revision A, 2023, released under DAA 20230007818.

[3] D. Saha, N. Bazmohammadi, J. M. Raya-Armenta, A. D. Bintoudi, A. Lashab, J. C. Vasquez, and J. M. Guerrero, "Space microgrids for future manned lunar bases: A review," *IEEE Open Access Journal of Power and Energy*, vol. 8, pp. 570–584, 2021.

[4] A. Lashab, M. Yaqoob, Y. Terriche, J. C. Vasquez, and J. M. Guerrero, "Space microgrids: New concepts on electric power systems for satellites," *IEEE Electrification Magazine*, vol. 8, no. 4, pp. 8–19, 2020.

[5] M. Yaqoob, M. Nasir, J. C. Vasquez, and J. M. Guerrero, "Self-directed energy management system for an islanded cube satellite nanogrid," in *IEEE Aerospace Conference*, 2020, pp. 1–7.

[6] M. Yaqoob, A. Lashab, J. C. Vasquez, J. M. Guerrero, M. E. Orchard, and A. D. Bintoudi, "A comprehensive review on small satellite microgrids," *IEEE Transactions on Power Electronics*, vol. 37, no. 10, pp. 12 741–12 765, 2022.

[7] P. A. Iles, "Evolution of space solar cells," *Solar Energy Materials and Solar Cells*, vol. 68, no. 1, pp. 1–13, 2001.

[8] R. R. King, D. C. Law, and K. M. E. et al., "40% efficient metamorphic gainp/gainas/ge multijunction solar cells," *Applied Physics Letters*, vol. 90, no. 18, p. 183516, 2007.

[9] X. Li, G. Li, H. Lu, and W. Zhang, "¿35% 5-junction space solar cells based on the direct bonding technique," *Journal of Semiconductors*, vol. 42, no. 12, pp. 123–129, 2021.

[10] A. Edpuganti, V. Khadkikar, M. S. Elmoursi, H. Zeineldin, N. Alsayari, and K. A. Hosani, "A comprehensive review on cubesat electrical power system architectures," *IEEE Transactions on Power Electronics*, vol. 37, no. 3, pp. 3161–3177, 2022.

[11] T. M. et al., "Simulation of a lunar surface base power distribution network for the constellation lunar surface systems," in *NASA Technical Report NASA/TM-2010-216084*, 2010.